Ultra-Low-Loss Hollow-Core Bragg Antiresonant Fiber With Super Bandwidth Transmission Window

Changming Xia, Zhipeng Deng, Aoyan Zhang, Peng Cai, Zhifeng Mo, Jiantao Liu, Guiyao Zhou, Zhiyun Hou, Qingmao Zhang, and Liang Guo

***Abstract*—A novel hollow-core antiresonant fiber with a Bragg structure is proposed. It is numerically simulated using a commercial finite element method, and optical properties of the fiber, such as mode field, confinement loss, and bend loss, are numerically analyzed. The proposed hollow-core antiresonant fiber has advantageous optical properties, such as ultralow confinement loss, large bandwidth, and low bend loss. The structural advantage of the hollow-core Bragg antiresonant fiber also facilitates the fabrication of long-distance hollow-core antiresonant fibers. Additionally, this fiber offers potential applications in long-distance communications, data transmission, and laser power delivery.**

***Index Terms*—Bragg antiresonant fiber, Ultra low loss, Bandwidth transmission window.**

I. Introduction

HOLLOW-CORE antiresonant fibers (HC-ARFs) with a negative core-cladding-interface curvature have been used in many fields and devices, including fiber optic gyroscopes [1], gas lasers [2], data transmission [3], sensors [4], high-power ultrashort pulse propagation, linear and nonlinear pulse propagation [5], and supercontinuum generation [6], [7]. Their excellent properties such as low loss, low dispersion, ultralow Brillouin scattering [8], exceptional polarization purity [9], a wide bandwidth transmission window, a large core, and single mode operation [10], [11] make them suitable for such applications. Recently, the performance of nested antiresonant nodeless fiber (NANF) has been improved considerably, and the loss of HC-ARF is being progressively minimized, and its length is increasing. In 2019, Bradley *et al.* reported a hollow-core NANF with a loss of 0.65 dB/km across the full C and L telecommunication bands [12]. The length of the fiber was up to 1.23 km, and it was in a single mode over sufficiently long lengths and could transmit data [12]. In 2020, Jasion *et al.* reported a 1.7-km hollow-core NANF with a low loss of 0.28 dB/km and wavelength range of 1510–1600 nm [13]. In the same year, Jasion reported advances in hollow-core NANFs with low optical losses of 2.8 dB/km and 1.23 dB/km at 650 nm and 1070 nm, respectively. In 2021, Sakr *et al.* reported a hollow-core NANF with 0.22 dB/km loss at 1300 nm and 1625 nm, respectively, using five nested tubes, and they achieved optical losses of 0.6 and 0.3 dB/km at 850 nm and 1060 nm, respectively. At present, the longest reported length of a hollow-core NANF is up to 2185 m [13]. It is also the longest hollow-core NANF reported so far. The loss of hollow-core NANFs is close to that of telecommunication optical fibers [14]. However, it is difficult to achieve lower loss and longer transmission distances for hollow-core NANFs, owing to their structure and fabrication technology [15]. For example, the reported cladding structure of hollow-core NANFs is almost a single nest with the support cladding of fiber, and a gas press is needed in the whole fiber-drawing process. Therefore, a novel hollow-core fiber structure is required to improve the loss and length of hollow-core NANFs. In early 2001, Johnson *et al.* reported a large-core omniguide fiber with omniguide cladding and low loss [16]. In 2004, Vienne *et al.* reported a new class of hollow-core Bragg fibers. The claddings of this Bragg fiber are composed of concentric cylindrical silica rings separated by nanoscale support bridges, and the bandwidth of the bandgap guiding of this Bragg fiber can exceed that of other hollow-core fibers. However, the loss of this Bragg fiber is large and up to 1 dB/m [17]. It is interesting that the structure of this optical fiber inspires a new idea to mitigate the existing problems of hollow-core fibers.

In this study, we proposed a novel HC-ARF with three concentric cylindrical silica capillary tube rings as the fiber cladding. Because these tubes represent a Bragg structure, we named this type of fiber a hollow-core Bragg antiresonant fiber (HC-BARF). The effect of the fiber structure on the confinement loss was numerically simulated using a commercial finite element method. The proposed HC-BARF may enable long-distance communications, data transmission, and laser-power delivery.

II. Structure Design of HC-BARF

Herein, a novel HC-ARF with a Bragg structure is proposed. Fig. 1 shows a cross section of the HC-BARF. As shown in Fig. 1, the cladding of the proposed fiber comprises three concentric

Manuscript received December 17, 2021; revised February 18, 2022; accepted March 3, 2022. Date of publication March 8, 2022; date of current version May 3, 2022. This work was supported in part by the Development Program in Key Areas of Guangdong Province under Grant 2018B010114002, and in part by the National Natural Science Foundation of China under Grant 61935010. *(Corresponding author: Changming Xia.)*

Changming Xia, Peng Cai, Qingmao Zhang, and Liang Guo are with the Guangdong Province Key Laboratory of Nano-Photonic Functional Materials and Devices, South China Normal University, Guangzhou, Guangdong 510006, China (e-mail: xiacmm@126.com; pcai@m.scnu.edu.cn; zhangqm@scnu.edu.cn; guoliangchn@163.com).

Zhipeng Deng, Aoyan Zhang, Zhifeng Mo, Jiantao Liu, Guiyao Zhou, and Zhiyun Hou are with the Guangzhou Key Laboratory for Special Fiber Photonic Devices and Applications, South China Normal University, Guangzhou, Guangdong 510006, China (e-mail: 1448543441@qq.com; 2019022157@m.scnu.edu.cn; 764445781@qq.com; liujiantao@hryh-fiber.com; gyzhou@scnu.edu.cn; houzhiyun@m.scnu.edu.cn).

Digital Object Identifier 10.1109/JPHOT.2022.3157264

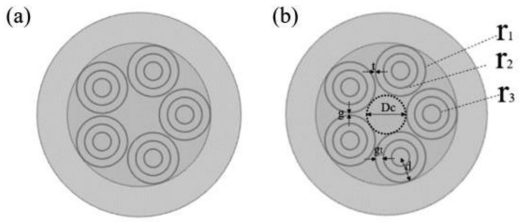

Fig. 1. Schematic of HC-BARF design with an ideal structure. (a) Across-section, (b) Structure parameters.

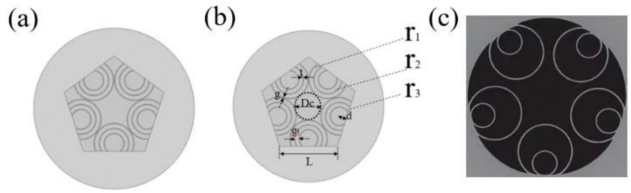

Fig. 2. Schematic of HC-BARF with real structure for fiber fabrication. (a) Across-section, (b) Structure parameters, (c) Cross-section of HC-ARF in previous literature [20].

cylindrical silica capillary tube rings surrounding an air core, which represent a Bragg structure. The outside radius of three concentric cylindrical silica capillary tube rings are r_1,r_2,r_3, respectively. The core diameter of the HC-BARF is *Dc*, and the thickness *t* of the cylindrical silica capillary tube is determined by the condition of antiresonance [18]. Furthermore, g_t is the gap between two concentric cylindrical silica capillary tube rings, r_1-t- g_t = r_2, r_2-t - g_t = r_3, *g* is the gap between two antiresonance tubes, and d is the distance between the cladding circle core and nested position.

As mentioned above, this structure is an ideal optical fiber structure. Through complex fiberend photonic devices based on the HC-ARF can be fabricated using 3D-printed waveguide technology [19]. However, an HC-BARF with an ideal structure is difficult to fabricate in the laboratory, owing to the lack of support for the inner cladding tubes r_2 and r_3. Therefore, the structure of HC-BARFs must be changed to fabricate this type of HC-BARF in the laboratory. We propose a novel HC-BARF structure, as shown in Fig. 2(a). Comparing structure of Fig. 2(a) with that of Fig. 2(c) reported in previous literature [20], it's not hard to find that, here, a pentagonal structure is utilized, which can effectively support the fiber cladding of three concentric cylindrical silica capillary tubes and maintain structural integrity for fiber fabrication. Based on the finite element method, the optical properties of the HC-BARF were numerically simulated using COMSOL Multiphysics (COMSOL Inc.). A 5-μm-thick perfectly matched layer (PML) was added. The maximum element size of the silica and air regions were $\lambda/5$.

III. Results and Discussion

A. Fundamental Mode and High-Order Fiber Modes

Fig. 3 shows the fundamental mode and high-order mode of the HC-BARF at wavelengths of 1550 and 1310 nm for L = 34 μm, g_t = 4.8 μm, r_1 = 16.5 μm, r_2 = 11.7 μm, r_3 = 6.9 μm, and t = 0.36 μm. As observed in Fig. 3, the HC-BARF

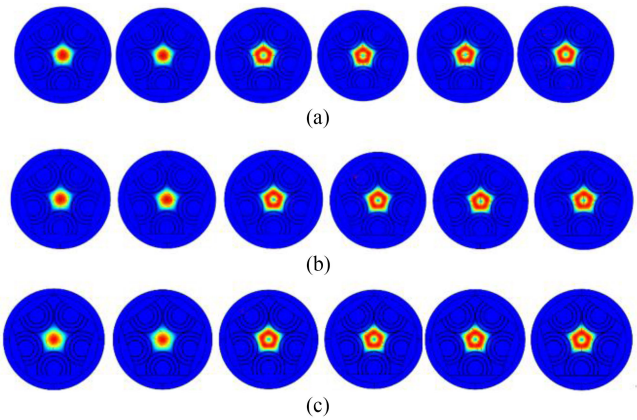

Fig. 3. Fundamental and high-order mode intensity distribution of HC-BARF at wavelengths of (a) 1550,(b) 1310 nm and (c) 1050nm, L = 34 μm, g_t = 4.8 μm, r_1 = 16.5 μm, r_2 = 11.7 μm, r_3 = 6.9 μm, t = 0.36 μm.

can support the transmission of the fundamental mode and many high-order modes. The main energy of the HC-BARF is concentrated in its air core.

B. Effect of Structure Parameters on Confinement Loss for Fixed Cladding Circle Center

Here, the centers of three concentric cylindrical silica capillary tube rings in the fiber cladding have the same position. Fig. 4 shows the effect of the structural parameters on the confinement loss, including structural parameters *Dc, g_t, g, d, L*. As shown in Fig. 4(a), when L = 34 μm, r_1 = 16.5 μm, g_t = 4.8 μm, and λ = 1550 nm, the confinement loss (*CL*) of the fiber first decreases and then increases with an increase in t. When t is approximately 0.35 μm, the *CL* of the fundamental mode is at its lowest. As shown in Fig. 4(b), when L = 34 μm, r_1 = 16.5 μm, g_t = 4.8 μm, and t = 0.36 m, the CL first decreases and then increases with increasing wavelength λ. The *CL* is at its lowest when the wavelength λ is approximately 1.05 μm. As shown in Fig. 4(c), when L = 34 μm, r_1 = 16.5 μm, t = 0.34 μm, and λ = 1550 nm, the *CL* first decreases and then increases with an increase in g_t. When g_t is approximately 4.75 μm, the *CL* of the fundamental mode is at its smallest. In addition, the effect of the inner pentagon side length of the optical fiber on the *CL* was also investigated. Here, the inner pentagon side length of the optical fiber determines the distance d between the cladding ring core and inner pentagon side. As observed in Fig. 4(d), when gt = 4.2 μm, t = 0.34 μm, and λ = 1550 nm, the CL decreases with an increase in the inner pentagon side length. Moreover, the CL decreases with an increase in r_1. When r_1 = 14.5 μm and L = 43 μm, the *CL* decreases below 10^{-2} dB/km, which is lower than that reported in previous literature [10]. The ultralow loss of HC-BARF facilitates its application in high-power laser delivery [21] and data transmission [22]. Using parameter optimization, the loss of HC-BARF can be further reduced.

C. Effect of Structure Parameters on CL for a Fixed Dc

All the fibers had the same core diameter of 35 µm. The effect of the structural parameters on the *CL* for a fixed *Dc* (*Dc* = 35 μm) in the proposed HC-BARF was investigated at 1550 nm

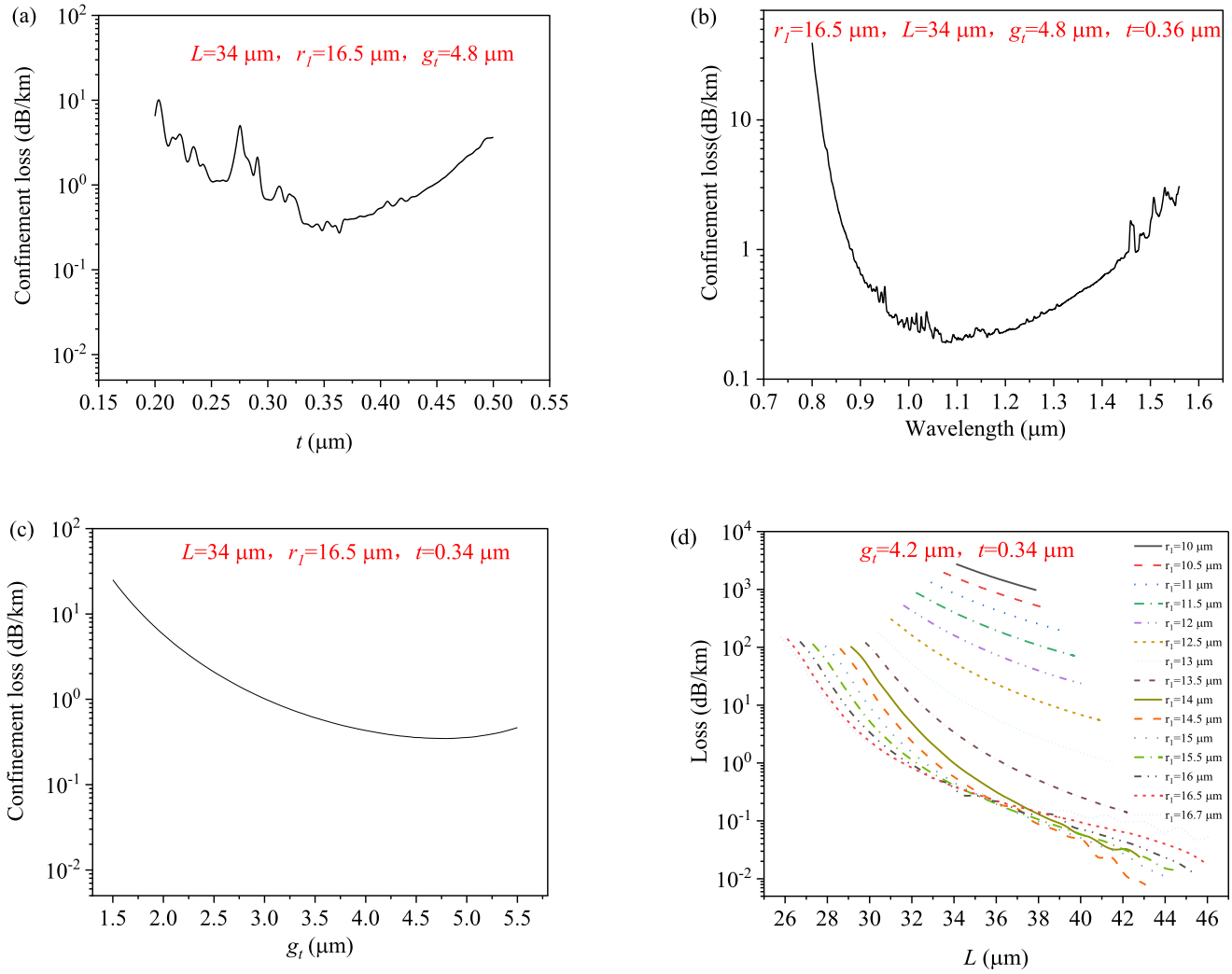

Fig. 4. CL spectrum for different structure parameters of the HC-BARF, including (a) t, (b) λ, (c) g_t, and (d) L and r_1.

and 1310 nm. *Dc* was determined according to the value reported in a previous study. The core center of the cladding silica ring is set through the center of the inner cladding ring to fabricate a long-distance fiber with a stable structure. As shown in Fig. 5(a), the *CL* first decreases and then increases with an increase in gt under $t = 0.34$ μm and $r_1 = 19$ μm. When g_t is approximately 5.5 μm, the *CL* is at its lowest. The CL is below 10^{-1} dB/km, which is lower than that reported in previous literature [10]. As shown in Fig. 5(b), for $r_1 = 19$ μm and $g_t = 5.4$ μm, when $t = 0.34$ μm, the *CL* is at its lowest value at approximately 10^{-2} dB/km. As shown in Fig. 5(c), for $g_t = 5.4$ μm and $t = 0.35$ μm, the *CL* decreases rapidly for $r_1 = 19$ μm when L ranges from 45 μm to 65 μm. According to the above analysis, the structure-optimization parameters of the HC-BARF are $r_1 = 19$ μm, $t = 0.35$ μm, and $g_t = 5.4$ μm. Moreover, when L is between 50 μm and 65 μm, *CL* is below 10^{-1} dB/km. As shown in Fig. 5(d), *CL* first decreases and then increases with an increase in the wavelength range from 0.8 μm to 1.6 μm. The *CL* is lower than 10^{-1} dB/km in the whole band. Moreover, the *CL* is at its lowest at approximately 1.05 μm and below 10^{-3} dB/km, which is lower than any value reported in previous literature [10]. The *CL* at 1050, 1064, 1310, and 1550 nm is 0.53×10^{-3}, 0.54×10^{-3},1.12×10^{-3}, and 4.92×10^{-3} dB/km respectively. Compared with the structure proposed in the previous literature [10]–[13], the structure proposed in this paper is advantages. The main reason is that fiber proposed in this paper combines anti resonance effect and Bragg effect, which reduce the loss of optical fiber [13], [16], [17]. As shown in Fig. 5d, the bandwidth of the transmission window in the HC-BARF is up to 800 nm, which is larger than that reported in previous literature [20], [23], 670 nm bandwidth is obtained in literature [23], and it can cover the entire O+S+C+L communication band (1.28-1.6 μm), which is basically consistent with that reported in the literature [24], [25],And our loss at is much lower than that reported in the literature [24]. Moreover, it is difficult to obtain long-distance long fiber in the laboratory for the complex structure of fiber reported in the literature [24]. In addition, the surface scattering loss (SSL) is calculated [23] because it is significant issue for hollow core fiber as shown in Fig. 5(d). As seen from Fig. 5(d), the SSL is smaller than 0.1dB/km over the wavelength of interest. The SSL of 1050,1064,1310, and 1550 nm is 0.06,0.056,0.022, and 0.02 dB/km, respectively.

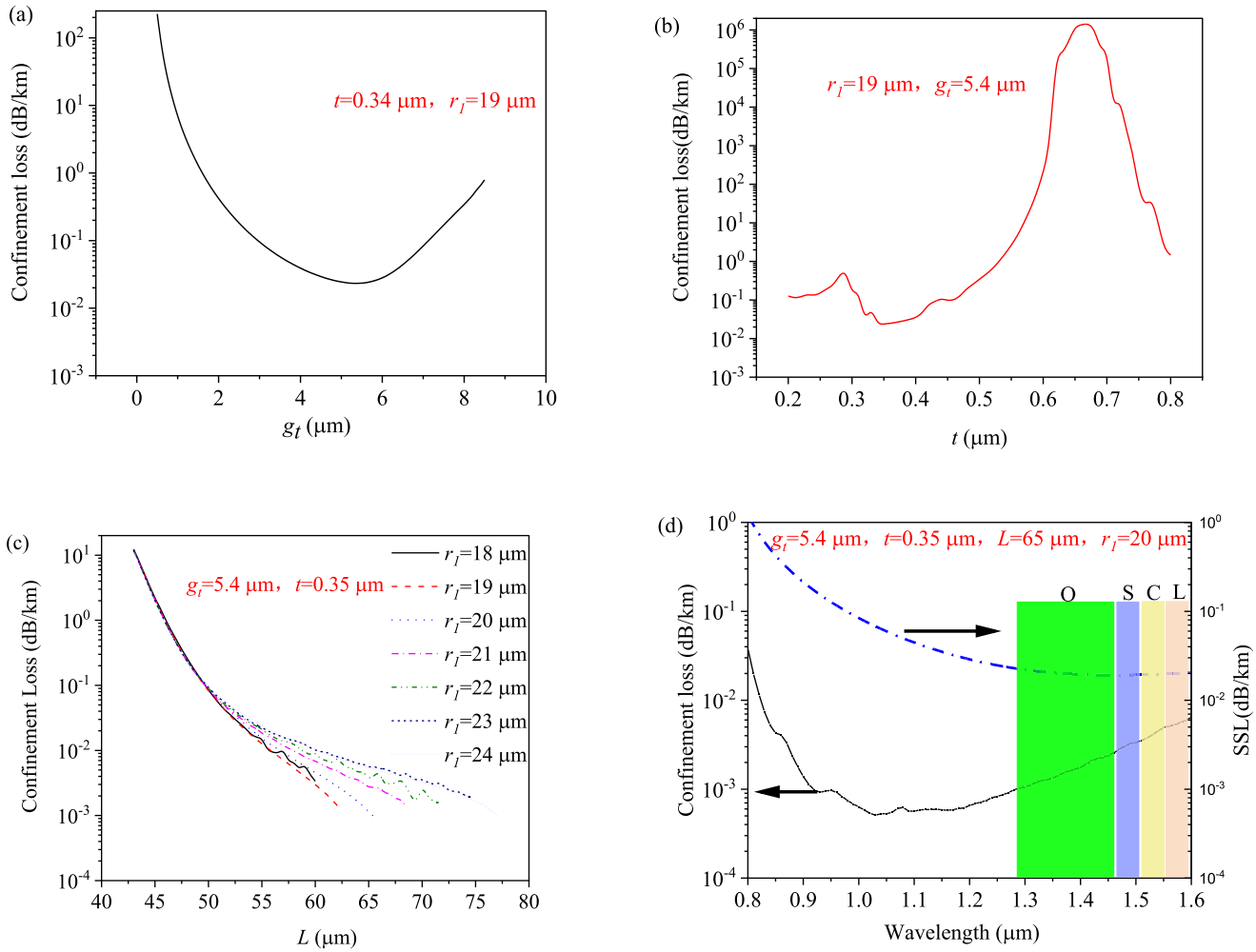

Fig. 5. *CL* spectrum for different structure parameters of the HC-BARF, including (a) g_t, (b) t, (c) L, and (d) λ and SSL is added.

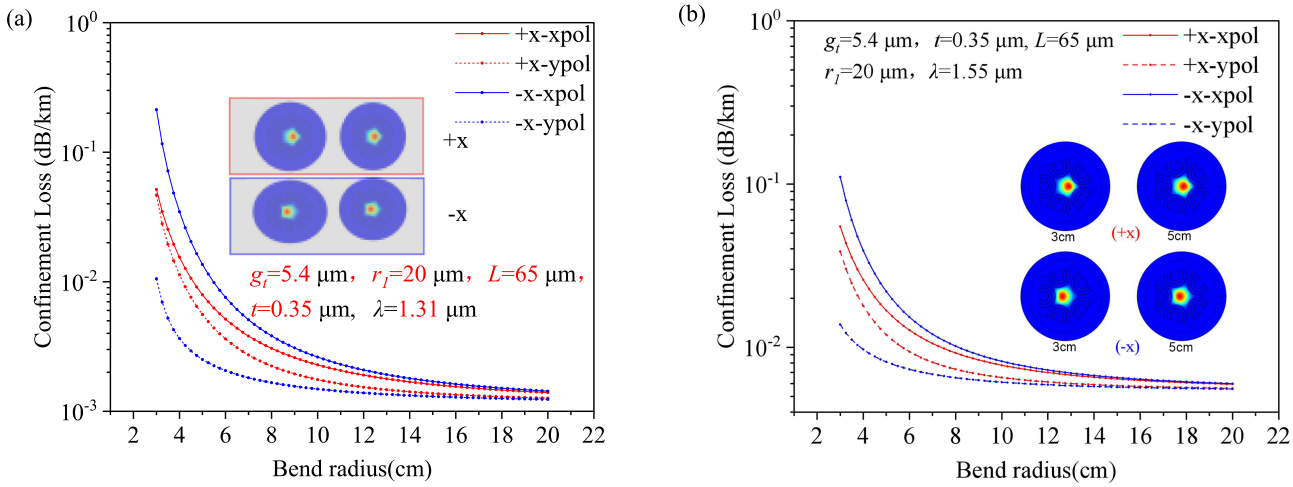

Fig. 6. CL spectrum for different bending diameters of HC-BARF under $g_t = 5.4\ \mu$m, $t = 0.35\ \mu$m, $L = 65\ \mu$m, and $r_1 = 20\ \mu$m for wavelengths of (a) 1310 nm and (b) 1550 nm.

D. Effect of Bend Radius on CL

HC-ARF length was reported up to 2185 m in 2021[10].However, according to current research progress, fiber length and bend loss are the most significant barriers to the application of HC-ARFs [15], [26], [27].Here, the structure of the proposed HC-BARF can be realized at a long distance; however, bend loss has a greater effect on the application of HC-BARF than the length of the fiber [27]. Therefore, according to the reference [28], [29], the bend loss of HC-BARF was studied using a commercial finite element method. As shown in Fig. 6, the bend loss increases with a decrease in the bend radius. For $g_t = 5.4$ μm, $r_1 = 20$ μm, $L = 65$ μm, and $t = 35$ μm, the bend loss at 1310 nm is lower than 10^{-2} dB/km when the bend radius is larger than 15 mm. Moreover, the bend loss at 1550 nm is lower than 10^{-1} dB/km when the bend radius is larger than 15 mm. A bend radius of 15 mm is smaller than that of a traditional optical fiber. Moreover, a loss of 10^{-1} dB/km does not affect the HC-BARF's application in the field of communication because this loss is lower than that of traditional communication optical fibers[14]. According to the above results, the proposed HC-ARF is a type of bending resistance fiber that can enable long-distance applications of optical fibers. As shown in the inset of Fig. 6, the optical field is confined to the air core of the fiber when the fiber is bent toward the X and Y axes.

IV. Conclusion

A novel HC-BARF with ultralow loss, super wideband, and antibending properties is proposed. This type of fiber can mitigate limitations such as short transmission distances, high loss, and high bend loss in reported antiresonant fiber [15], [30]. The results show that HC-BARF has ultralow loss ranging from 800 nm to 1600 nm, and the *CL* is lower than 10^{-1} dB/km. The CL at approximately 1050 nm is the lowest at a value below 10^{-3} dB/km. Moreover, the bandwidth of the transmission window in HC-BARF is up to 800 nm, which can cover the entire O+S+C+L communication band. The fiber has a small bend radius of 15 mm, which is smaller than the 19 mm bend radius of traditional optical fibers used for communication. Thus, the proposed HC-BARF offers potential applications in long-distance communications, data transmission, and laser power delivery. In the future, we will study HC-BARFs fabricated using a 3D printed technology in our laboratory.

References

[1] G. Sanders, A. Taranta, C. Narayanan, E. N. Fokoua, and D. Payne, "A hollow-core resonator fiber optic gyroscope using nodeless anti-resonant fiber," *Opt. Lett.*, vol. 46, no. 1, pp. 46–49, 2020.

[2] M. Xu, F. Yu, and K. Jonathan, "Mid-infrared 1W hollow-core fiber gas laser source," *Opt. Lett.*, vol. 42, no. 20, pp. 4055–4058, 2017.

[3] X. C. Wang, D. W. Ge, W. Ding, Y. Y. Wang, and P. Wang, "Ultralow loss hollow-core conjoined-tube negative-curvature fiber for data transmission," in *Proc. Opt. Fiber Commun. Conf.*, 2019, pp. 1–3.

[4] I. M. Ankan, M. A. Mollah, J. Sultana, and M. S. Islam, "Negative curvature hollow-core anti-resonant fiber for terahertz sensing," *Appl. Opt.*, vol. 59, no. 28, pp. 8519–8525, 2020.

[5] S. Wu, B. Siwicki, R. M. Carter, F. Biancalana, and D. P. Hand, "Impact of nonlinear effects on transmission losses of hollow-core anti-resonant negative-curvature optical fiber," *Appl. Opt.*, vol. 59, no. 16, pp. 4988–4996, 2020.

[6] Y. P. Yatsenko *et al.*, "Multiband supercontinuum generation in an air-core revolver fibre," *Quantum Electron.*, vol. 47, no. 6, pp. 553–560, 2017.

[7] M. I. Hasan, N. Akhmediev, and W. Chang, "Mid-infrared supercontinuum generation in supercritical xenon-filled hollow-core negative curvature fibers," *Opt. Lett.*, vol. 41, no. 21, pp. 5122–5125, 2016.

[8] A. Iyer, W. Xu, J. E. Antonio-Lopez, R. A. Correa, and W. H. Renninger, "Ultra-low Brillouin scattering in anti-resonant hollow-core fibers," *APL Photon.*, vol. 5, no. 9, 2020, Art. no. 096109.

[9] A. Taranta, E. N. Fokoua, S. Mousavi, J. R. Hayes, and F. Poletti, "Exceptional polarization purity in antiresonant hollow-core optical fibers," *Nat. Photon.*, vol. 14, pp. 504–510, 2020.

[10] B. Xza *et al.*, "5-tube hollow-core anti-resonant fiber with ultralow loss and single mode," *Opt. Commun.*, vol. 501, 2021, Art. no. 127347.

[11] M. S. Habib, J. E. Antonio-Lopez, C. Markos, A. Schulzgen, and R. A. Correa, "Single-mode, low loss hollow-core anti-resonant fiber designs," *Opt. Exp.*, vol. 27, no. 4, pp. 3824–3836, 2019.

[12] T. Bradley, G. Jasion, J. Hayes, Y. Chen, and F. Poletti, "Antiresonant hollow core fibre with 0.65 dB/km attenuation across the c and l telecommunication bands," in *Proc. 45th Eur. Conf. Opt. Commun.*, 2019, pp. 1–4.

[13] G. T. Jasion, T. Bradley, K. Harrington, H. Sakr, and F. Poletti, "Hollow core NANF with 0.28 dB/km attenuation in the c and l bands," in *Proc. Opt. Fiber Commun. Conf.*, 2020, pp. 1–3.

[14] Y. Tamura *et al.*, "The first 0.14-dB/km loss optical fiber and its impact on submarine transmission," *J. Lightw. Technol.*, vol. 36, no. 1, pp. 44–49, 2018.

[15] P. Poggiolini and F. Poletti, "Opportunities and challenges for long-distance transmission in hollow-core fibres," in *Proc. Opt. Fiber Commun. Conf.*, 2021, pp. 1-3.

[16] I. Johnson *et al.*, "Low-loss asymptotically single-mode propagation in large-core omniguide fibers," *Opt. Exp.*, vol. 9, no. 13, pp. 748–779, 2001.

[17] G. Vienne *et al.*, "Ultra-large bandwidth hollow-core guiding in all-silica Bragg fibers with nano-supports," *Opt. Exp.*, vol. 12, no. 15, pp. 3500–3508, 2004.

[18] N. M. Litchinitser, A. K. Abeeluck, C. Headley, and B. J. Eggleton, "Antiresonant reflecting photonic crystal optical waveguides," *Opt. Lett.*, vol. 27, no. 18, pp. 1592–1594, 2002.

[19] A. Bertoncini and C. Liberale, "3D printed waveguides based on photonic crystal fiber designs for complex fiber-end photonic devices," *Optica*, vol. 7, no. 11, pp. 1487–1494, 2020.

[20] H. Sakr *et al.*, "Hollow core NANFs with five nested tubes and record low loss at 850, 1060, 1300 and 1625 nm," in *Proc. Opt. Fiber Commun. Conf.*, 2021, pp. 1-3.

[21] A. V. Newkirk, J. M. Mercado, E. Antonio-Lopez, R. A. Correa, and A. Schulzgen, "High power laser delivery using anti-resonant hollow core fiber," in *Proc. Adv. Mater. Innovations Device Appl. XV*, 2021, Art. no. 118260D.

[22] Z. Liu *et al.*, "Nonlinearity-free coherent transmission in hollow-core antiresonant fiber," *J. Lightw. Technol.*, vol. 37, no. 3, pp. 909–916, 2019.

[23] A. Khaleque K.Shaha and M. S. Hosen, "Wideband low loss hollow core fiber with nested hybrid cladding elements," *J. Lightw. Technol.*, vol. 39, no. 20, pp. 6585–6585–6591, 2021.

[24] K. Shaha, A. Khaleque, and M. I. Hasan, "Low loss double cladding nested hollow core antiresonant fiber," *OSA Continuum*, vol. 3, no. 9, pp. 2512–2524, 2020.

[25] Md. Imran *et al.*, "Positive and negative curvatures nested in an antiresonant hollow-core fiber," *Opt. Lett.*, vol. 42, no. 4, pp. 703–706, 2017.

[26] J. R. Hayes, F. Poletti, and D. J. Richardson, "Reducing loss in practical single ring antiresonant hollow core fibres," in *Proc. Eur. Conf. Lasers Electro-Opt.*, Paper CJ2-2, 2011.

[27] W. Belardi and J. C. Knight, "Hollow antiresonant fibers with low bending loss," *Opt. Exp.*, vol. 22, no. 8, pp. 10091–10096, 2014.

[28] B. Yang, X. Liu, W. Jia, S. Liu, and Z. Wang, "Low loss hollow-core connecting-circle negative-curvature fibres," *IEEE Photon. J.*, vol. 13, no. 1, Feb. 2021, Art no. 7200710.

[29] S. Gao, Y. Wang, W. Ding, Y. Hong, and P. Wang, "Conquering the rayleigh scattering limit of silica glass fiber at visible wavelengths with a hollow-core fiber approach," *Laser Photon. Rev.*, vol. 14, 2020, Art. no. 1900241.

[30] M. C. Richard, "Measurement of resonant bend loss in anti-resonant hollow core optical fiber," *Opt. Exp.*, vol. 25, no. 17, pp. 20612–20621, 2017.